

Functional properties of nanocrystalline, submicrocrystalline and polygonized Ti-Ni alloys processed by cold rolling and post-deformation annealing

V.Brailovski^a, S.Prokoshkin¹, K.Inaekyan and V.Demers

Ecole de Technologie Supérieure, Montreal, Canada

¹ Moscow Institute of Steel and Alloys, Russia

Abstract. Thermomechanical processing consisting of cold rolling ($\epsilon=0.3-2.0$) and post-deformation annealing (300-450°C, 1h) was applied to binary Ti-Ni alloys to produce nanocrystalline structures (NS) or polygonized dislocation substructures (PDS), or their mixture. The evolution of the material structure and properties was studied using TEM, X-ray, microhardness, calorimetry and tensile testing techniques. Recovery stress and strain of the 50.26at%Ni alloy and superelastic strain of the Ti-50.6at%Ni alloy were measured under static and fatigue conditions.

It was found that higher true yield stress of NS alloys not only increases the recovery stress potential, but, since it is combined with a relatively low transformation yield stress; it increases the completely recoverable strain. NS alloys generate recovery stresses that are twice as high as those of PDS alloys (1200 MPa), completely recoverable strains that are 10% greater (up to 6% in tension), and they demonstrate a higher cyclic stability of functional properties. This improvement comes with the cost of a lower NS alloy fatigue damage tolerance, aggravated by the presence of microcracks caused by cold working. Binary Ti-Ni alloys, processed by annealing of an intermediately cold-worked ($\epsilon=0.75...1$) alloy and containing mixed nanocrystalline structure and polygonized dislocation substructure, allow a high fatigue life combined with relatively high and cyclically stable functional properties.

1. Introduction

The vast majority of bulk metallic materials with conventional coarse-grained structure can be severely deformed at low temperatures to refine their microstructure and produce ultrafine-grained and partially amorphized materials [1]. One of the numerous severe plastic deformation (SPD) technologies, cold rolling (CR), can be used to tailor specific microstructures in Ti-Ni shape memory alloys, ranging from a dislocation-hardened substructure to ultrafine-grained and partially amorphized structures, when cold-work strain increases from moderate (true strain $\epsilon=0.3-0.5$) to severe ($\epsilon=1.5-2$). A mixed amorphous/nanocrystalline structure issued from severe CR processing can be transformed into a nanocrystalline structure, after an appropriate post-deformation annealing (PDA). It has been shown that nanostructured Ti-50at%Ni alloy with 50 to 100 nm grain size confers significantly higher maximum recovery stress and maximum completely recoverable strain than a polygonized substructure with the same subgrain size [2]-[3]. The improvement of both the completeness of shape recovery and the recovery stress generation is attributed to the combination of a high true yield stress and a low transformation onset stress due to the particular dislocation-free nanocrystalline structure created by CR+PDA processing.

Recent work has shown that severe cold rolling conditions should be optimized because there is an increased risk of the appearance of rolling-related defects such as surface and edge cracks [4]. This is a classical trade-off situation: the higher the cold rolling intensity, the finer the material structure and the higher the functional properties of Ti-Ni shape memory alloy (SMA), but this improvement is reached in tandem with a greater the risk of microcrack appearance and therefore, a lower fatigue resistance [5]. This article focuses on the advantages and limitations of the CR-PDA technique, applied to binary Ti-Ni SMA, by comparing their single cycle and multiple cycle shape memory and superelastic properties.

^a e-mail: vbrailovski@mec.etsmtl.ca

2. Methodology

Two binary Ti-Ni shape memory alloys in the form of $\varnothing 1$ mm wire (Special Metals Corp., NY, USA): high-temperature Ti-50.26at%Ni alloy for actuator applications and low-temperature Ti-50.6at%Ni alloy for superelastic applications, were subjected to 1 to 6 passes of cold rolling: logarithmic thickness reduction: $e = 0.3$ to $e = 2.0$ (Ti-50.26at%Ni) and $e = 0.3$ to $e = 1.4$ (Ti-50.6at%Ni). Rolling was conducted with a constant speed of 30 mm/s using a FENN four-high laboratory rolling mill (5.6 KW DC motor) with pulling tension set at 10% of the true yield stress. The cold-rolled strips were then annealed at $T_{PDA} = 350, 400$ and 450°C (1 hour), where $T_{PDA} = 400^\circ\text{C}$ was selected as the reference annealing temperature because it corresponds to the best suited annealing temperature from the functional properties perspective [3].

The structure and substructure evolution was studied using a Tesla BS-540 transmission electron microscope. Thin foils were prepared using the “window” technique and electrolytic polishing in an $\text{HClO}_4 + \text{CH}_3\text{COOH}$ solution. Characteristic temperatures were measured using a Perkin Elmer DSC (see Table 1). Mechanical characterization was carried out using microhardness (Instron Tukon, 500g) and tensile testing (Enduratec ELF 3200 and MiniBionix MTS) techniques. To characterize the Ti-50.26at%Ni alloy performances as actuator material, corresponding samples were then subjected to thermomechanical cycling using a custom-made test bench [5], whereas to characterize the Ti-50.6at%Ni alloy performances as superelastic material, they were mechanically cycled at a constant temperature $T_d = A_f + 10^\circ\text{C}$.

Table 1. Temperatures of the direct (reverse) martensitic transformation: (A) Ti-50.26at%Ni and (B) Ti-50.6at%Ni

(A)Ti-50.26at%Ni		Direct transformation				Reverse transformation	
		Degrees Celsius					
e	T _{PDA}	M _f	M _s	R _f	R _s	A _s	A _f
quenched		44	57	N/A	N/A	76	93
0.25	400	-10	Cannot be separated		59	55	86
0.75		Thermally-induced martensitic transformation cannot be observed down to -150°C		48	59	55	81
1				50	59	43	73
1.5				49	59	38	68
2				49	59	38	65

(B)Ti-50.6at%Ni		Direct transformation				Reverse transformation	
		Degrees Celsius					
e	T _{PDA}	M _f	M _s	R _f	R _s	A _s	A _f
quenched		-6	4	N/A	N/A	21	37
0.25	400	Thermally-induced martensitic transformation cannot be observed down to -150°C		40	59	45	60
0.75				41	62	43	63
1				42	63	45	65
1.4				48	63	46	64

Testing of Ti-50.26at%Ni alloy as actuator material

The functional properties of SMA as an actuator material reflect its potential to generate recovery stresses and strains upon heating. To evaluate the SMA capacity to generate mechanical work, the following three-mode testing procedure is devised (Fig. 1.):

- Stress-free recovery mode:** An SMA specimen is first deformed at $T < M_f$, then released to allow an elastic springback with a martensitic strain ε_m (O-A-B-C, Fig. 1, a). The SMA specimen is then heated up to $T > A_f$ to transform the material from martensite to austenite and to regain its undeformed length (C-D). The SMA's martensitic (ε_M), austenitic (ε_A) and recovery ($\varepsilon_r = \varepsilon_M - \varepsilon_A$) strains are extracted. The cycle is repeated up to failure or run-out at 10^4 cycles. The test is interrupted if the value of the austenitic strain (ε_A) is close to that of the initial martensitic strain (ε_M). The results obtained are reported in Fig. 5a-c.
- Fixed-support recovery mode:** An SMA specimen is deformed at a temperature $T < M_f$, then released to allow an elastic springback, secured at its extremities at an initial martensitic strain ε_m (O-A-B-C) and heated up to $T > A_f(\sigma)$ (C-E), where $A_f(\sigma)$ is the final temperature of the reverse martensitic transformation under stress (Fig. 1. b). The recovery stress generated upon heating is defined as $\sigma_r = \sigma_A - \sigma_M$, where σ_A are austenitic and σ_M martensitic stresses, respectively. The constraint specimen is thermally cycled between room temperature

and an imposed heating temperature, up to specimen failure or test run-out at $22 \cdot 10^3$ cycles. For each test, to obtain different recovery stresses, the heating temperature is varied between 70 and 250°C. The results obtained are reported in Fig. 5d-f.

- C. *Constant-stress recovery (or stress-assisted two-way shape memory) mode*: An SMA specimen is deformed at a temperature $T < M_f$ by using a suspended weight (O-A-F), and then heated up to $T > A_f(\sigma)$ (F-G) (Fig. 1☼, c). After each heating-cooling cycle, the SMA's martensitic (ϵ_M), austenitic (ϵ_A) and recovery ($\epsilon_r = \epsilon_M - \epsilon_A$) strains are measured. The applied stress is adjusted to reach the end of the transformation stress plateau and corresponds to an initial strain of $5.7 \pm 0.5\%$. The loaded specimen is thermally cycled up to specimen failure or test run-out at $22 \cdot 10^3$ cycles. For each test, to obtain different recovery strains, the heating temperature is varied between 70 and 250°C. The results are reported in Fig. 5g-i.

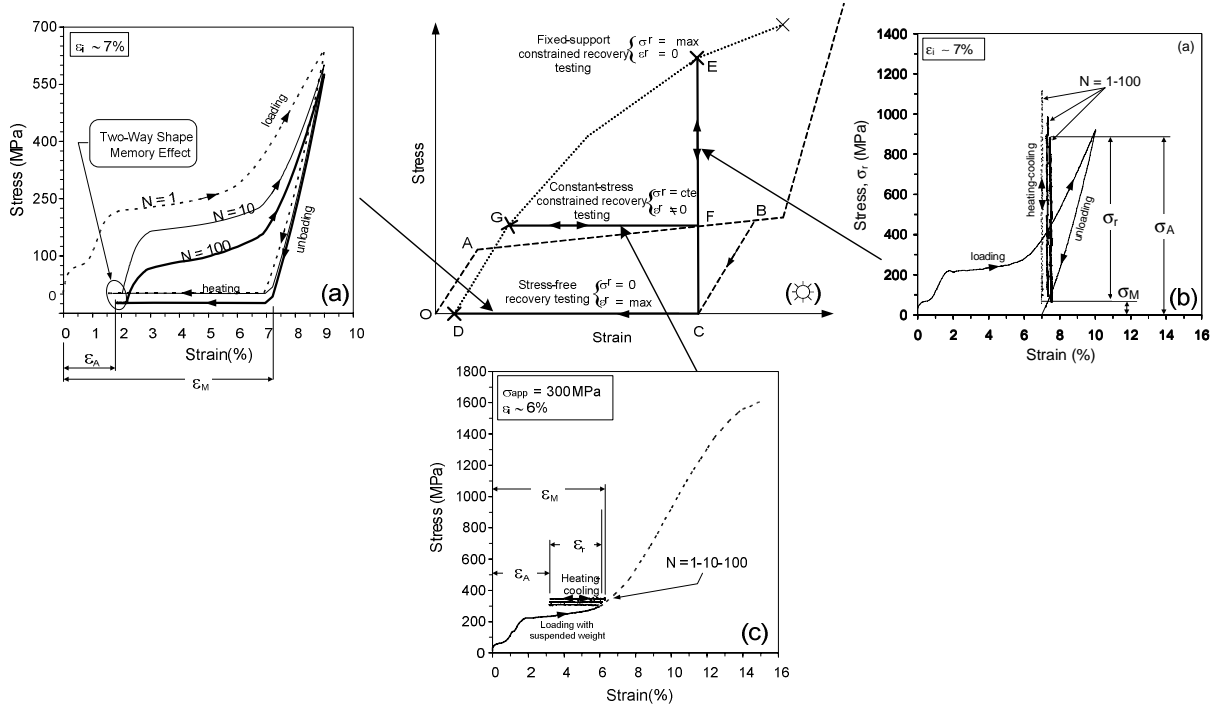


Fig. 1. Schematics of the strain-stress space (☼) and typical stress-strain diagrams for constant-stress recovery (a), fixed-support recovery (b) and stress-free recovery (c) testing modes.

The results obtained from all three testing modes allow the working space of a given active element to be delimited for variable bias conditions; the D-G-E curve determining the SMA element's equilibrium position in its austenitic state.

Testing of Ti-50.6at%Ni alloy as superelastic material

Tensile testing of the thermomechanically processed Ti-50.6at%Ni alloy samples is performed at $T = A_f + 10^\circ\text{C}$. During the first cycle, the 70 mm sample is stretched up to a maximum strain of 5%. This stretched length is maintained invariant during cycling. To completely describe the a superelastic loop, the following characteristic parameters must be used: upon loading, onset (start) $\sigma_s^{A \rightarrow M}$ and final $\sigma_f^{A \rightarrow M}$ stresses of the direct austenite-to-martensite transformation and corresponding strains ($\epsilon_s^{A \rightarrow M}, \epsilon_f^{A \rightarrow M}$); upon unloading, onset (start) and final stresses of the reverse martensite-to-austenite transformation and corresponding strains; and, finally, residual strains caused by material degradation (ϵ_d) (all from Fig. 2). From these characteristic points on the superelastic curve, Young modules for both austenite and martensite single phase material and stress-hardening coefficients for the direct and reverse transformations can be determined. In this study, the evolution of only two characteristics will be illustrated: the onset direct transformation stress $\sigma_s^{A \rightarrow M}$ and the residual strain due to material degradation ϵ_d .

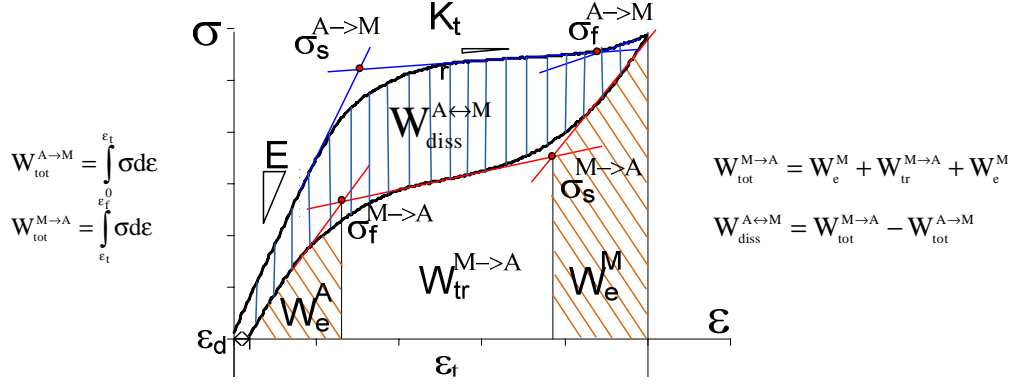


Fig. 2. Schematic superelastic strain-stress diagram

To evaluate the performance of the Ti-50.6at%Ni alloy as a spring material capable of accumulating and releasing mechanical energy, some additional parameters must be calculated: the energy accumulated upon loading $W_{tot}^{A \rightarrow M}$ and the energy restored upon unloading $W_{tot}^{M \rightarrow A}$. The latter has three components: the energy restituted due to mainly single phase martensite (W_e^M) and to single phase austenite (W_e^A) elastic recovery, and the energy restituted through transformation-related recovery mechanisms $W_{tr}^{M \rightarrow A}$. The difference between the accumulated and restored energies, $W_{diss}^{A \leftrightarrow M} = W_{tot}^{A \rightarrow M} - W_{tot}^{M \rightarrow A}$, corresponds to the energy dissipated during reversible B2 \leftrightarrow B19' transformation and is due to internal friction related to the interface movement. It should be noted that the level of the dissipated energy assumes its real significance when a particular application is contemplated. If the alloy is used for its damping capacities, the energy dissipated during cycling should be maximized, whereas if it is intended to be used as a spring element, a dental arch for example, it should be minimized. In this work, to reflect the efficiency of the superelastic element as a spring material, a coefficient η is introduced:

$$\eta = 1 - W_{diss}^{A \leftrightarrow M} / W_{tot}^{A \rightarrow M} \quad (1)$$

3. Results

3.1 Microstructural analysis

In Fig. 3, TEM bright- and dark-field images and selected area diffraction patterns are presented for Ti-50.26at%Ni alloys subjected to $\epsilon=0.3, 0.75, 1.5$ and 1.9 , with post-deformation annealing at 400°C (1 hour). The higher the cold-work intensity before annealing, the higher the quantity of B2-austenite and the smaller the R-phase structures and amount of martensite. After $\epsilon=1.9 + T_{PDA}=400^\circ\text{C}$ processing, mainly austenite structure and substructure are observed.

After ($\epsilon=0.3 + T_{PDA}=400^\circ\text{C}$) processing, martensite and R-phase structures, as well as a relatively small quantity of austenite structure with high dislocation density are observed. Diffraction spots are fragmented, broadened in the azimuthal direction (because of the involved imperfectness of crystallographic orientation across selected area) and in the radial direction (because of a significant increase in dislocation density). Subgrains of 15 to 100 nm are observed in the dark-field image (Fig. 3a). This is a polygonized dislocation substructure.

After ($\epsilon=0.75 + T_{PDA}=400^\circ\text{C}$), mixed submicrocrystalline polygonized structures and nanocrystalline structures are observed: in the dark-field image, the areas containing individual nanocrystals alternate with submicro-sized conglomerates of submicrograins. Asimuthal broadening of the diffraction spots becomes more pronounced than after initial $\epsilon=0.3$, thus reflecting a greater crystallographic misorientation of substructural elements across the selected area (Fig. 3b).

After ($\epsilon=1.5 + T_{PDA}=400^\circ\text{C}$), the structure contains evenly distributed austenite nanograins with dimensions varying from 30 to 60 nm and a small quantity of polygonized substructure, the latter witnessed by the presence of subgrains similar to those located in the middle of the Fig. 3c bright-field image. On the dark-field image, a certain number of distinct grains can clearly be seen. Diffraction rings in this case contain overlapping but distinct spots from different grains of the structure and strongly azimuthally and radially broadened diffraction spots superposed from misoriented subgrains of the polygonized substructure (Fig. 3c).

After ($\epsilon=1.9 + T_{PDA}=400^{\circ}\text{C}$), the structure is almost completely nanocrystalline. Radial broadening of the diffraction spots becomes less pronounced, thus reflecting lesser dislocation density in the material and therefore a decreasing quantity of the polygonized substructure in favour of a larger quantity of the nanocrystalline structure (Fig. 3d).

Note that the same microstructural changes can be observed in Ti-50.6at%Ni alloy, but, given the higher precipitation activity in this nickel-rich compound, thermally-activated processes such as static recovery, polygonization (in moderately deformed alloy), or crystallization and grain growth (in severely deformed alloy) are shifted to higher annealing temperatures.

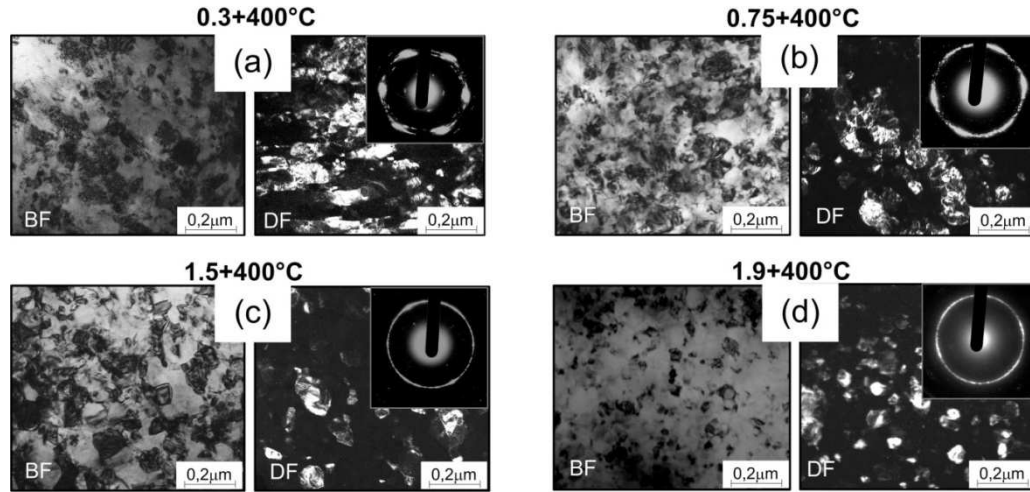


Fig. 3. Transmission electron microscopy (BF – bright-field, DF – dark-field) of Ti-50.26at%Ni alloy subjected to cold rolling $\epsilon = 0.3$ (a), 0.75 (b), 1.5 (c) and 1.9 (d) and post-deformation annealing at 400°C . Electron diffraction patterns are inserted.

3.2 Mechanical properties of the thermomechanically-processed binary TiNi alloys

The evolution of the RT-tested mechanical properties of Ti-50.26at%Ni alloy in respect to the logarithmic thickness reduction is presented for the cold-rolled material in Fig. 4a, and for the cold-rolled and annealed material ($T_{PDA} = 400^{\circ}\text{C}$, 1 hour) in Fig. 4b. In the first case, stress-induced martensitic transformation cannot be observed and the stress-strain curves are similar to those of common low-ductility alloys. In the second case, the onset stress for the martensite reorientation $\sigma_s^{A \rightarrow M}$, yield stress (YS) and ultimate tensile stress (UTS) can be measured. It can be observed that the higher the logarithmic thickness reduction, the higher all the mechanical characteristics, but the increase in YS is more significant than that of $\sigma_s^{A \rightarrow M}$, which forecasts improving functional properties of the alloy. However, an important scatter in tensile characteristics is observed for logarithmic thickness reductions exceeding $\epsilon=1.2$ (70%), related to the increased level of the cold-work and the corresponding higher probability of microcracking [4]. The latter phenomenon considerably risks impairing the fatigue properties of the alloys.

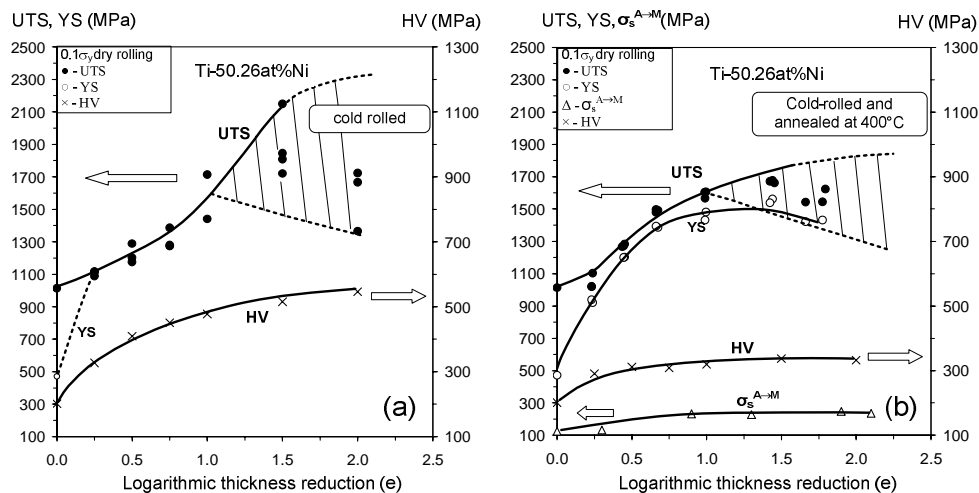


Fig. 4. Mechanical properties vers. the cold-work for the a) cold-rolled and b) cold-rolled and annealed Ti-50.26at%Ni alloy

3.3 Ti-50.26at%Ni alloy as actuator material

Typical testing curves are presented in Fig. 5a-i for the stress-free, fixed-support and constant-stress recovery modes for $e = 0.75, 1$ and 1.5 cold work intensities. In every case, when thermomechanical cycling is repeated, an evolution of the material behavior is observed.

A. Stress-free recovery

The higher the cold work intensity, the greater the stability of the strain recovery behavior, but this positive effect is reached at the expense of a decrease in the specimens' life (Fig. 5a,b,c).

B. Fixed-support recovery

The higher the cold work intensity, the higher the maximum recovery stress generated during the 1st heating-cooling cycle, but this gain rapidly attenuates as the number of the stress recovery cycles increases. Furthermore, the higher the cold work intensity, the lower the recovery stress that can be sustained for the run-out number of thermomechanical cycles $N = 22 \cdot 10^3$ (Fig. 5d,e,f).

C. Constant-stress recovery

During constant-stress recovery testing, contrary to two previous testing modes, recovery forces and displacement are generated simultaneously, and their product corresponds to the mechanical work produced by an SMA element during cycling. Higher cold work intensity corresponds to greater alloy stability and higher stresses generated for the same level of recovery strains, which result in more mechanical work produced during one heating-cooling cycle. This positive effect is, however, counterweighted by a shorter fatigue life and, therefore, by a smaller total amount of mechanical work produced by the specimen till failure (Fig. 5g,h,i).

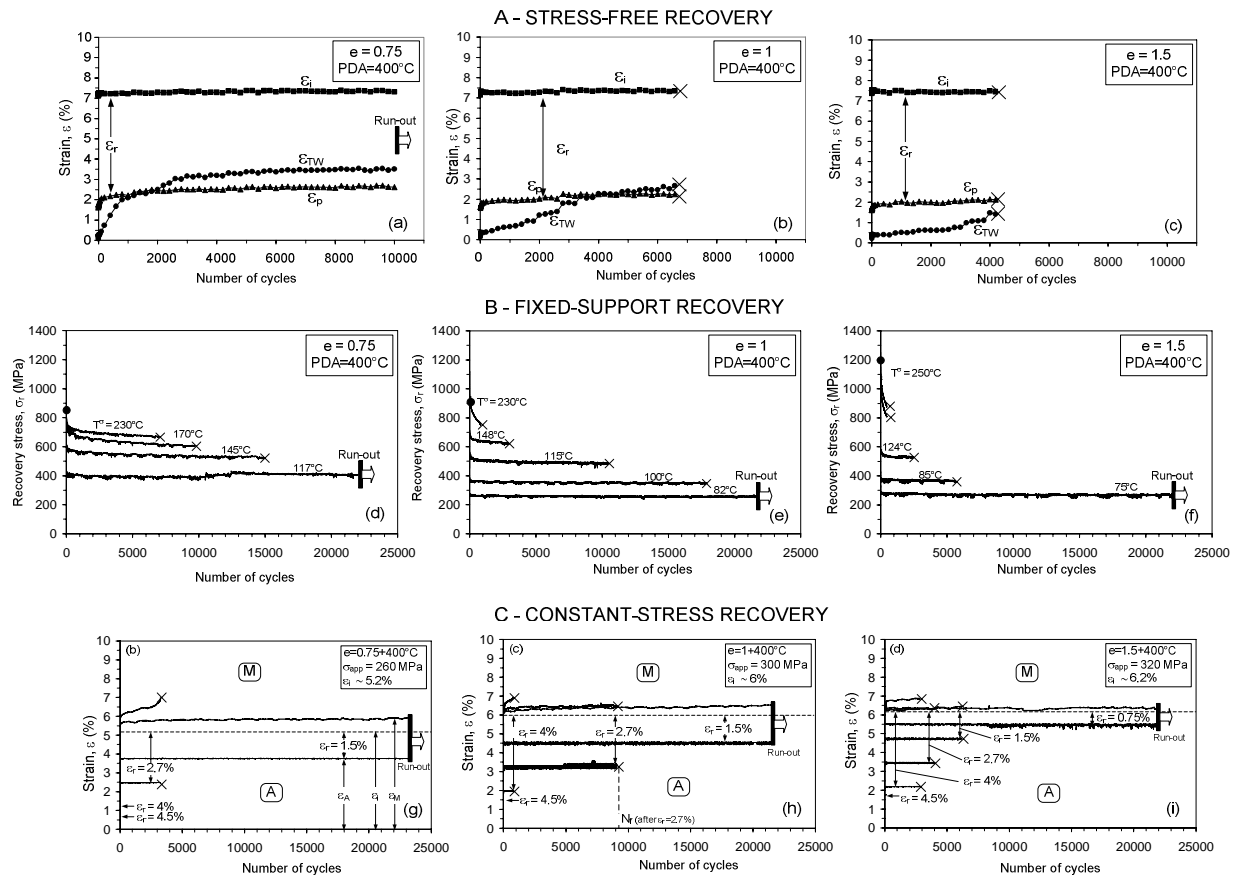


Fig. 5. A - stress-free recovery (a), (b) and (c); B - fixed-support recovery (d), (e) and (f); C - constant-stress recovery (g), (h) and (i); $e = 0.75$ (a), (d), (g), $e = 1$ (b), (e) and (h); $e = 1.5$ (c), (f) and (i) (adapted from [5]).

In Fig. 6 and in Table 2, the results obtained for all of the cold work conditions ($e = 0.3, 0.75, 1.0, 1.5$ and 1.9) are collected for comparison purposes. The results from the stress-free recovery mode are plotted on the abscissa of the combined recovery stress-strain diagram (Fig. 6, $\varepsilon \neq 0, \sigma = 0$); those from the fixed-support recovery mode, on the ordinate ($\sigma \neq 0, \varepsilon = 0$), and the results from the constant-stress recovery mode are shown with the $\sigma \neq 0, \varepsilon \neq 0$ coordinates.

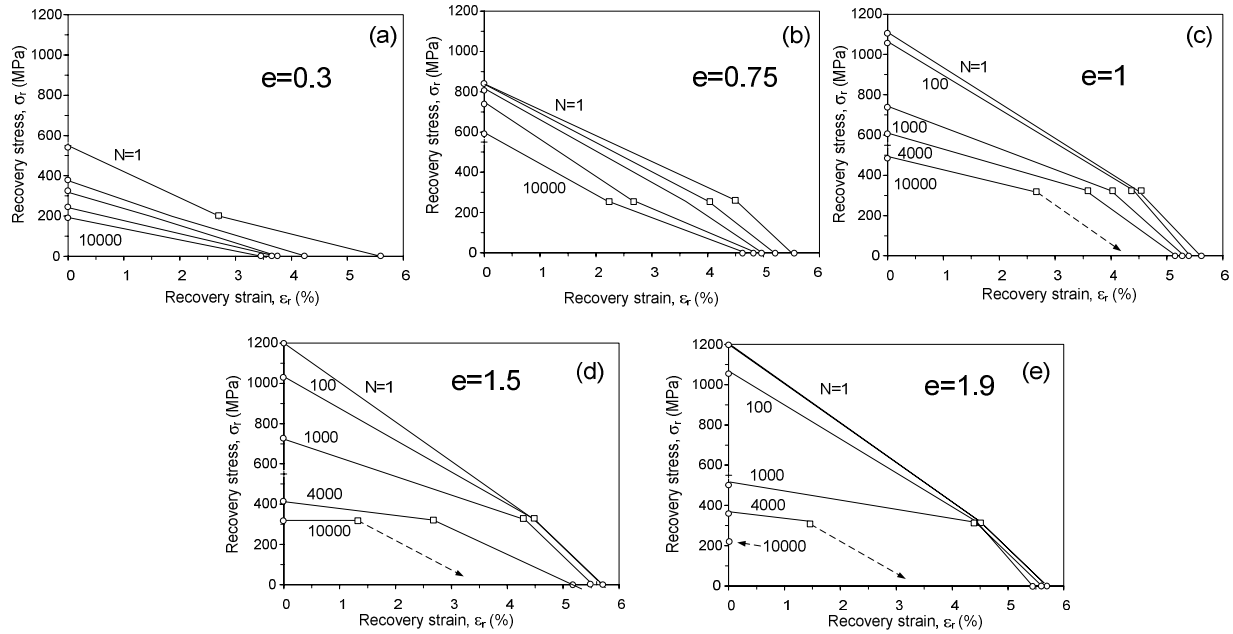


Fig. 6. Combined recovery stress-strain diagrams for different processing conditions of Ti-50.26at%Ni alloy: $e=0.3$ (a), 0.75 (b), 1.0 (c), 1.5 (d), 1.9 (e).

Table 2. Results of single and multiple-cycle testing of Ti-50.26at%Ni alloy as actuator material

Cold work strain	Single-cycle testing		Multiple-cycle testing (fatigue)					
			Stress-free recovery		Fixed-support recovery		Constant-stress recovery	
	Recovery stress (MPa)	Recovery strain (%)	Recovery strain (%)	N before failure	Run-out stress, MPa	N run-out, 10^3 cycles	Work/cycle MJ/m^3	Total work GJ/m^3
0.3	560	4	4	Rut-out at 10000	195	22	6	11
0.75	850	5.3	4.5	Rut-out at 10000	400	22	10	128
1.0	1100	5.5	5	6500	270	22	13	120
1.5	1250	5.9	5.4	4000	280	22	14	75
1.9	1400	6	5.8	1200	250	22	15	25

It can be observed that the higher the cold-work intensity, the larger the recovery stress-strain envelopes corresponding to low-cycle fatigue life, but, as the number of cycles increases, this work generation potential shrinks faster than that corresponding to lower cold-work intensities; the best compromise being $e = 1 + T_{\text{PDA}} = 400^\circ\text{C}$ processing, which results in a mixed polygonized-nanocrystalline microstructure (Fig. 6). It should be noted that the working envelopes corresponding to severe cold working conditions could be significantly enlarged if the technological processing becomes more defect-free. To address this problem, the use of shape instead of flat cold rolling and the application of proper post-annealing finishing technologies such as mechanical polishing can be envisaged.

3.4 Ti-50.6at%Ni alloy as superelastic material

Superelastic curves obtained with Ti-50.6at%Ni alloy samples tested at $A_f + 10^\circ\text{C}$ are presented in Fig. 7, and the onset stresses and residual strains are plotted as functions of the number of cycles in Fig. 8. It can be observed that the higher the cold work intensity and the lower the annealing temperature, the higher the onset stresses of the direct martensitic transformation, which is well known [6]. As far as stability of the superelastic behaviour is concerned, the higher the cold work intensity and the lower the annealing temperature, the lower the residual

strain accumulation and the onset stress decrease with cycling, but this higher stability is reached at the expense of the specimen's cyclic life (Fig. 7, Fig. 8). In contrast, with low-intensity cold work ($\epsilon=0.3$), the material degradation was so significant that testing had to be interrupted before failure occurred.

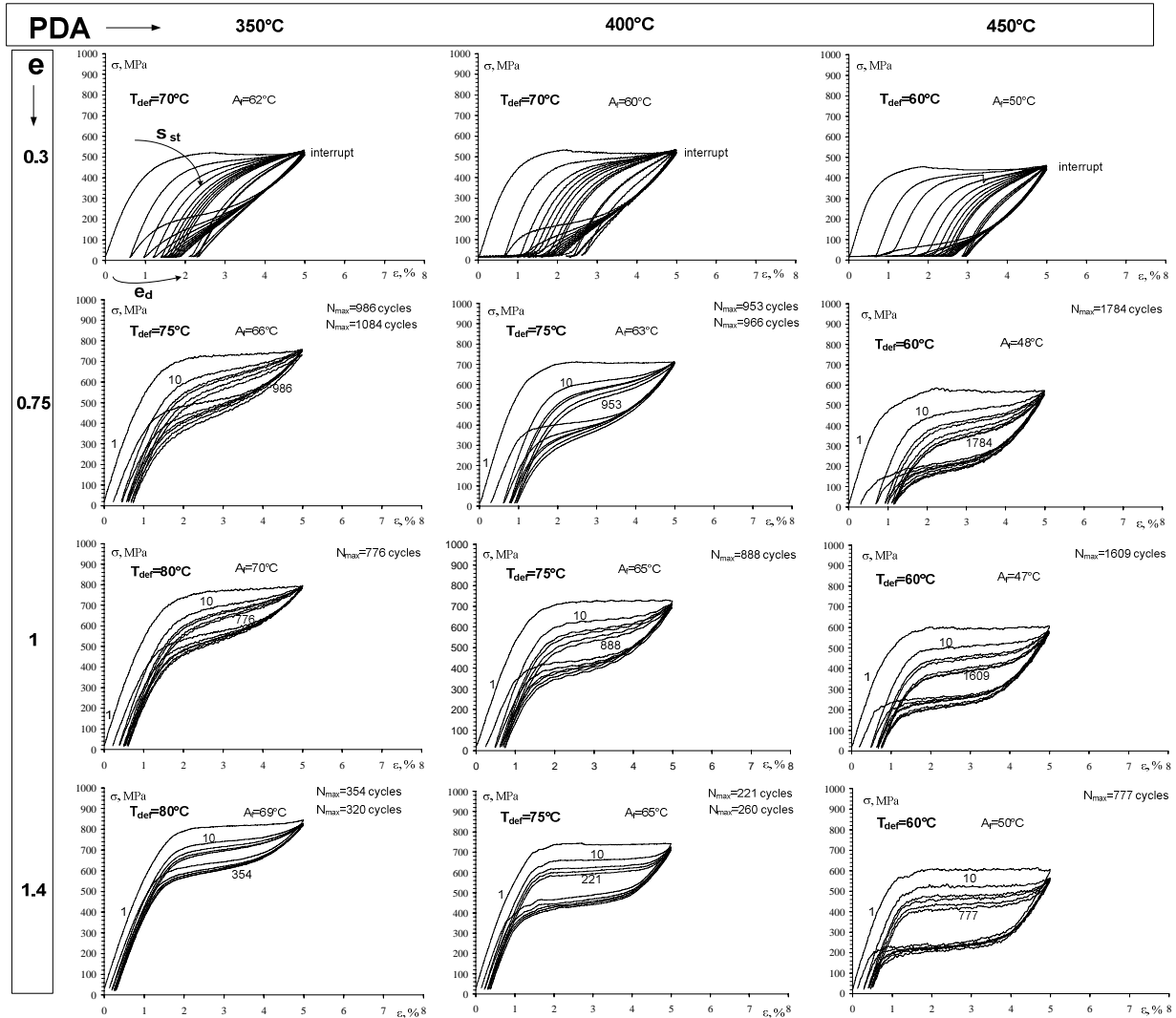


Fig. 7. Superelastic curves of Ti-50.6at%Ni alloy for $\epsilon = 0.3, 0.75, 1$ and 1.4 (rows) and $T_{PDA} = 350, 400, 450^\circ\text{C}$ (columns). Arrows on the $\epsilon = 0.3, T_{PDA} = 350^\circ\text{C}$ diagram indicate increase in number of cycles.

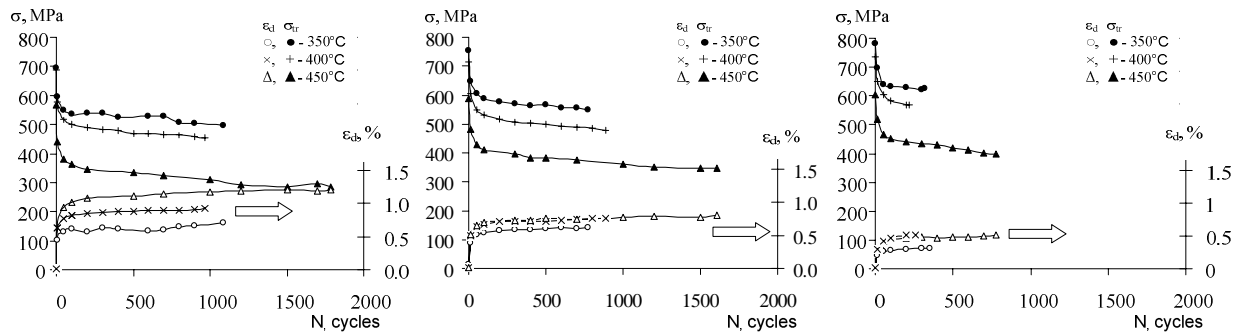


Fig. 8. Direct transformation onset stresses and residual strains as functions of the number of cycles: a) $\epsilon = 0.75$, b) $\epsilon = 1$, c) $\epsilon = 1.4$

In Fig. 9, three mechanical energy components are plotted in respect to the thermomechanical processing conditions (see Fig. 2 for definition): energy corresponding mainly to the elastic recovery of the single martensite (W_e^M) and austenite (W_e^A) phases, transformation-related energy recovered ($W_{tr}^{M \rightarrow A}$), and energy dissipated during superelastic loading and unloading ($W_{diss}^{A \leftrightarrow M}$). Note that the sum of these components corresponds to the total mechanical energy accumulated in the material during superelastic loading ($W_{tot}^{A \rightarrow M}$). These results are presented in Fig. 9a,b,c for single cycle testing (10th cycle is taken) and in Fig. 9d,e,f, for multiple cycle testing where the energy components are summarized for all the cycles before failure.

For the single-cycle testing, it can be observed that the higher the cold-work intensity and the lower the PDA temperature, the greater the overall mechanical energy involved in cycling, mostly because of the higher onset stresses in these cases. The quantity of dissipated energy appeared to be strongly affected by the annealing temperature – the higher the annealing temperature, the greater the dissipated energy – while being less significantly affected by the cold-work intensity. These phenomena result in the highest energy restitution efficiency for the case of $e=1.4 + T_{PDA}=350^\circ\text{C}$ ($\eta=0.9$, see equation (2) and Table 3).

In the case of multiple-cycle testing, however, the situation becomes inversed: the higher the cold-work intensity, the lower the overall mechanical energy accumulated and restituted during cycling, mostly due to the lower number of cycles associated with this processing. As for the influence of the annealing temperature, the situation becomes complex because the lowest mechanical energy corresponds to an intermediate 400°C and not to a lower 350°C annealing temperature. This intermediate temperature affects all of the cold-work intensities, reflecting the adverse influence of the intensive Ti_3Ni_4 precipitation at 400°C on the fatigue resistance during superelastic cycling. The results obtained for single and multiple-cycle superelastic testing of Ti-50.6at%Ni alloy samples are collected in Table 3.

To summarize, it can be observed that the higher the cold-work intensity, the larger the energy accumulation/restitution potential of the alloy, but, as the number of cycles increases, this potential decreases faster than that corresponding to lower cold-work intensities; the best compromise being $e=0.75 \dots 1.0 + T_{PDA}=400^\circ\text{C}$ processing, which results in a mixed polygonized-nanocrystalline microstructure.

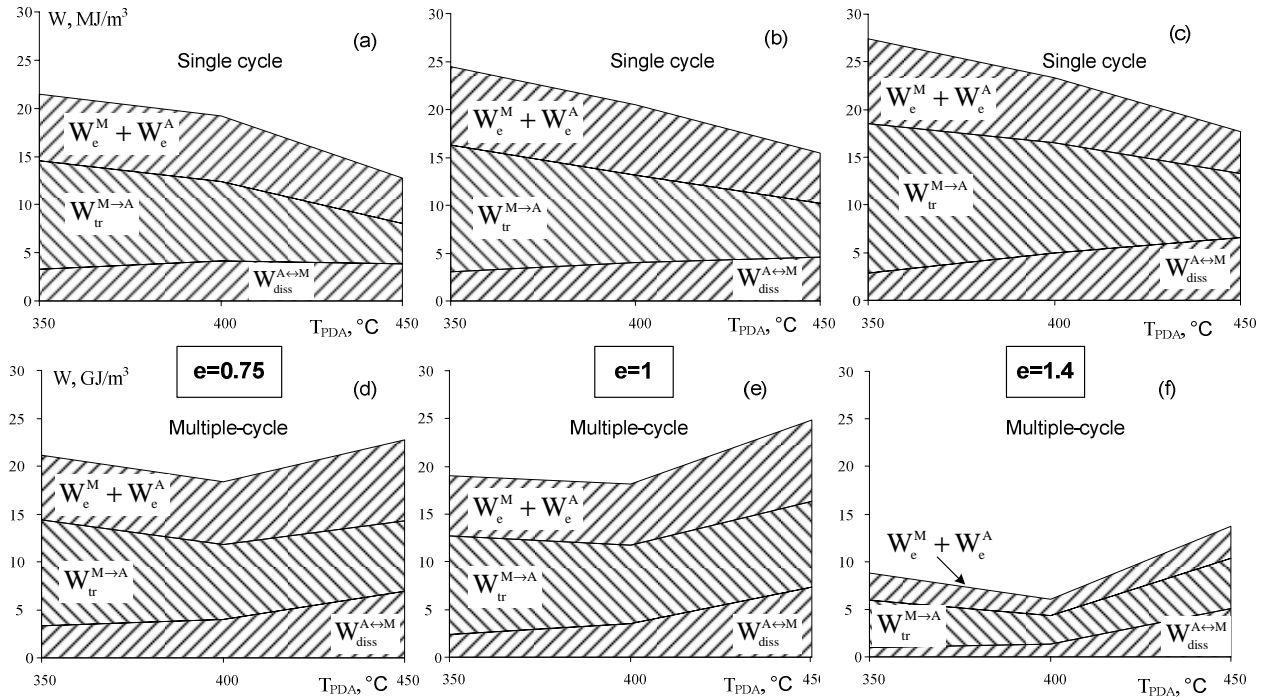


Fig. 9. (a-c) Energy components per cycle (cycle 10 is taken) and (d-f) energy components per lifespan as functions of the thermomechanical processing.

Table 3. Results of single and multiple-cycle testing of Ti-50.6at%Ni alloy as superelastic material

		Single-cycle testing			Multiple-cycle testing (fatigue)											
		Accum. strain*, %			Accum. strain* (%)			N before failure			Energy/cycle, MJ/m ³ Total energy, GJ/m ³			Energy restitution efficiency		
T _{PDA} , °C		350	400	450	350	400	450	350	400	450	350	400	450	350	400	450
Cold work strain	0.3	0.7	0.75	0.8	2.2	2.7	3	cycle interrupted before failure (significant accumulated strain)								
	0.75	0.3	0.32	0.35	0.8	0.9	1.2	1000	960	1800	22/22	19.5/19	15/23	0.85	0.78	0.72
	1.0	0.22	0.25	0.25	0.6	0.78	0.81	780	890	1600	25/19	20/18	17/25	0.88	0.81	0.71
	1.4	0.1	0.15	0.15	0.3	0.4	0.5	350	240	780	27/8	24/7	19/14	0.90	0.78	0.63
* Total initial strain for the 1 st cycle is 5%																

4. Conclusions

1. By increasing the cold rolling thickness reduction from $e = 0.3$ to 1.9 (Ti-50.26at%Ni) and from $e = 0.3$ to 1.4 (Ti-50.6at%Ni), it becomes possible – after post-deformation annealing at $350, 400, 450^{\circ}\text{C}$ (1 hour) – to regulate the material microstructure from a polygonized substructure to a nanocrystalline structure, passing through a mixed polygonized-nanocrystalline microstructure.
2. During single-cycle testing, shape memory (stress and strain generation) and superelastic (reversible deformation) properties reach their absolute maximum in alloys with nanocrystalline structure due to a unique combination of a high true yield stress and a low transformation onset stress in these materials.
3. During multiple-cycle testing, nanocrystalline alloys demonstrate higher cyclic stability in their functional properties than mixed polygonized-nanocrystalline alloys, but lower fatigue resistance, mainly because of the cold-work induced defects.
4. If an application engineer requires alloys with the highest stress-strain recovery potential and functional stability, but only for a limited number of cycles, nanocrystalline alloys are the best solution. However, alloys with mixed polygonized-nanocrystalline microstructure ($e=0.75-1.0 + T_{\text{PDA}}=400^{\circ}\text{C}$) represent an interesting compromise in terms of the best possible combination of functional performance, cyclic stability and fatigue resistance.

Acknowledgement

The authors would like to thank the Natural Sciences and Engineering Research Council of Canada and the Federal Agency for Education of the Russian Federation for their financial support.

References

- [1] E.V. Tatyannin and V.G. Kurdyumov: Physica status solidi (a) 121 (1990) pp. 455-462.
- [2] Prokoshkin, S., Brailovski, V., Khmelevskaya, I. Yu. et al, Metal Science and Heat Treatment, V.47, No 5-6, 2005, pp. 182-187.
- [3] V. Brailovski, S. Prokoshkin, I.Yu. Khmelevskaya et al, Materials Trans. JIM, 47 (2006), 795-804.
- [4] V. Demers, V. Brailovski, S. Prokoshkin, and K. Inaekyan, Journal of Materials Processing Technology, 209 (2009), 3096-3105.
- [5] V. Demers, V. Brailovski, S. Prokoshkin, and K. Inaekyan, Mater. Sci. Eng. A, 513-514 (2009), 185-196.
- [6] Miyazaki S., Engineering aspects of shape memory alloys, Edit. Duerig T.W. et al, Butterworth-Heinemann, London, 1990, pp. 394-413